scientific reports

Check for updates

OPEN

Panax notoginseng saponins suppress the PI3K/AKT pathway to enhance autophagy and apoptosis in pulmonary fibrosis

Jiong Hou[1,2,4], Lei Li[1,4], Chun-bin Sun[1,4], Tian-gang Li[1], Si-qi Zhang[1], Peng-tao Liang[1], Yan-ling Jin[1], Jia-li Yuan[1], Li Li[1], Jin-yuan Yan[3]✉, Yi Fu[1]✉ & Zhong-shan Yang[1]✉

The progressive development of pulmonary fibrosis (PF) is accompanied by an exaggerated inflammatory response and the accumulation of extracellular matrix in the lung parenchyma. *Panax notoginseng* saponins (PNS) exert promising anti-fibrotic effects involving a cross-talk between autophagy and apoptosis. However, the mechanisms underlying the effects of PNS are yet to be elucidated. In this study, PNS significantly reduced inflammatory injury and collagen deposition in the lungs of PF mice, simultaneously increasing the expression of autophagy-associated and pro-apoptotic genes and the number of autophagosomes and apoptotic bodies. Notably, when either autophagy or apoptosis was inhibited, collagen accumulation was observed. This suggests that both cellular processes independently contribute to the therapeutic effects of PNS. Additionally, while autophagy blockade disruption apoptosis activation, autophagy function remained independent of apoptosis. Network pharmacology and molecular docking analyses showed the PI3K-AKT signal pathway mediating efficacy. The targets included HSP90AA1, MAPK1, STAT3, EGFR, and HIF1A. Furthermore, PNS suppressed the PI3K-AKT signal pathway to modulate autophagy and apoptosis both in vivo and in vitro. Collectively, our findings demonstrate that PNS is a putative therapeutic option in PF that acts via the PI3K-AKT signaling pathway to modulate autophagy and apoptosis. Targeting the cellular degradation machinery is a viable therapeutic strategy for PF.

Keywords Pulmonary fibrosis, Collagen deposition, *Panax notoginseng* saponins, Autophagy, Apoptosis, PI3K/AKT

Abbreviations

α SMA	Alpha smooth muscle actin
AMPK	AMP-activated protein kinase
ATG	Autophagy-related gene
COL-I	Collagen type I
COL-III	Collagen type III
ECM	Extracellular matrix
EGFR	Epidermal growth factor receptor
ESR1	Estrogen receptor 1
GRB2	Growth factor receptor-bound protein 2
GSK3β	Glycogen synthase kinase 3 beta
HIF1A	Hypoxia-inducible factor 1 alpha
HSP90AA1	Heat shock protein 90 alpha family class A member 1
KDR	Kinase insert domain receptor
LC3	Microtubule-associated protein 1 light chain 3
MAPK1	Mitogen-activated protein kinase 1

[1]Yunnan Key Laboratory of Integrated Traditional Chinese and Western Medicine for Chronic Disease in Prevention and Treatment, Yunnan University of Chinese Medicine, Kunming 650500, China. [2]College of Life Sciences, Anhui Medical University, Hefei 230032, China. [3]Central Laboratory, Kunming Medical University Second Hospital, Kunming 650500, China. [4]Jiong Hou, Lei Li, Chun-bin Sun contributed equally to this work. ✉email: yanjinyuan@kmmu.edu.cn; fukeyi_27@163.com; yangzhongshan@ynucm.edu.cn

mRNA	Messenger ribonucleic acid
PARP	Poly (ADP-Ribose) polymerase
PF	Pulmonary fibrosis
PI3K	Phosphoinositide 3-kinase
PNS	*Panax notoginseng* saponins
p38/JNK/MAPK	p38 C-Jun N-terminal kinase/mitogen-activated protein kinase
STAT3	Signal transducer and activator of transcription 3
TGF β1	Transforming growth factor beta 1

Pulmonary fibrosis (PF) is a widespread, non-specific lung condition characterized by alveolar inflammation and interstitial PF, which has a protracted course and a poor prognosis[1]. Although the mechanisms underlying fibrosis in PF are yet to be elucidated, a hypothesis on PF pathogenesis caused by recurrent injuries is currently favored, and this has been deemed as the originator for sensitive predisposed alveolar epithelium[2,3]. Progressive damage was found to induce an aberrant repair response characterized by the multiplication of initiator fibroblasts and their conversion into myofibroblasts. This resulted in ECM overaccumulation and collagen deposition, which consequently induced or exacerbated PF[4].

Earlier research has indicated the presence of autophagy in PF[5,6]. Autophagy, often known as "self-eating", is an evolutionarily conserved mechanism. It involves the phagocytosis and degradation of damaged organelles, lipid droplets, and macromolecular aggregates through the lysosomal degradation pathway, which is essential for preserving homeostasis[7,8]. Microtubule-associated protein 1 light chain 3 (LC3), a traditional marker for autophagy, is localized to the membrane of double-membraned autophagosomes[9]. When LC3 II binds to autophagy receptors, it targets autophagic lysosomes. This process is catalyzed by the autophagy-related protein 12 (ATG12) complex[10]. In PF, autophagy is markedly inhibited, along with a concomitant decline in the quantity of autophagosomes. Mice with the autophagy gene *ATG7* knocked out were shown to exhibit greater susceptibility to bleomycin (BLM)-induced PF, with a significant increase in the levels of accumulated collagen[11,12]. Rapamycin, an autophagy inducer, has been confirmed to facilitate autophagy by hindering the mTOR pathway, which consequently delays PF[13]. Autophagy possibly plays a crucial role in helping prevent PF.

Apoptosis is a conserved mechanism of cellular destruction that plays an essential role in PF pathophysiology[14]. It is a strictly controlled process leading to cell death, comprising cell membrane shrinkage, nuclear pyknosis, membrane blebbing, and other cellular changes. In promoting self-destruction, cells are decomposed into apoptotic bodies, which are subsequently phagocytized by the surrounding cells[15]. Both endogenous and exogenous apoptosis are activated and initiated by a family of cysteine proteases known as caspases, which are the central regulators of apoptosis[16]. The impairment of myofibroblast apoptosis may induce a repair process, culminating in PF[17]. Apoptosis avoidance has emerged as a characteristic feature of fibrotic disorders, which eventually results in the development of a senescent phenotype[14]. The self-destruction machinery, which is geared toward apoptosis, participates in PF. Apoptosis and autophagy are self-destructive mechanisms that contribute to numerous diseases. The management of both processes requires interaction between the anti-apoptotic proteins Bcl-2 and Beclin 1[18]. However, the precise mechanism underlying this cross-talk remains unclear. In our study, we focused on identifying crucial mediators between autophagy and apoptosis in disease states.

P. notoginseng (Burkill) F.H. Chen [Araliaceae], popularly known as Sanqi, is a traditional herb widely cultivated in the central and eastern regions of Yunnan Province, China, an ideal growing area. It is a key ingredient in several traditional Chinese medicine formulations, including Dan Shen Dropping Pills and Yunnan Baiyao[19]. Previous studies have shown that *P. notoginseng* possesses anti-inflammatory, antioxidant, and anti-fibrotic properties and can inhibit fibroblast activation, thereby improving fibrosis occurring in different organs[20–22]. *Panax notoginseng* saponins (PNS), as the chief constituent of *P. notoginseng*, have been historically used in various preparations in treating cancer and conditions of the respiratory, circulatory, and metabolic systems. It is widely used in medical research and clinical applications[23]. In recent times, scientists have focused on the role of PNS in anti-pulmonary fibrosis[24], including its role in PF attenuation via the regulation of the renin-angiotensin system[25]. However, to our knowledge, comprehensive studies have not been conducted on the protective effects of PNS active ingredients on PF and the underlying mechanisms, especially those mediated via self-destructive processes. This topic warrants further investigation[26,27]. According to recent research, the PI3K/AKT signaling cascade is integral to the pathophysiology of PF and has promising targets for therapeutic intervention. The abnormal activation of this signaling pathway has been connected to heightened fibroblast proliferation, differentiation, and resistance to programmed cell death, which complicates the fibrotic process[28,29].

We intended to explore the therapeutic effects of PNS in PF and the underlying mechanisms. The ameliorating effects of PNS on inflammatory damage and collagen deposition in PF were first confirmed in human lung fibroblasts (HLFs). The data obtained demonstrated the importance of PNS in triggering the autophagic machinery to resist PF. Our findings offer a fresh perspective on the multifaceted effects of PNS in PF, highlighting its potential for regulating the PI3K/AKT pathway and essential processes in autophagy and cell death. Our research contributes to a deeper understanding of the pathogenesis of PF, providing a rationale for potential therapeutic interventions in PF.

Results

Impact of PNS on lung injury improvement in mice with PF

The primary pathological characteristic of PF is excessive inflammation accompanied by collagen deposition[30–32]. H&E and Masson's trichrome staining tests were conducted to assess the impact of PNS on lung injury in mice with PF. Severe morphological and structural damage in the tissues was observed in the BLM model group. The damage caused included alveolar septal widening, alveolar wall rupture, alveolar fusion, and inflammatory

cell infiltration, along with ECM deposition (Fig. 1A). However, following treatment with PNS for 28 days, the damage caused to the alveolar structure was found to be ameliorated, and the alveolar wall was remodeled. Specifically, a decrease in inflammatory cell infiltration was observed. Compared to that in the model group, ECM deposition and the fibrous area were notably reduced in a dose-dependent manner in groups treated with PNS at doses of 50, 100, and 200 mg/kg/day ($P < 0.05$). The pulmonary coefficient was significantly lower in the PNS-treated group compared to the model group (Fig. 1C). Body weight in the PNS-treated group was significantly higher than that of the model group (Fig. 1E). The level of hydroxyproline, a key marker for PF, showed significant concentration-dependent reduction in lung tissues compared to that in the model group (Fig. 1D). Restrictive ventilatory dysfunction, characterized by reduced lung adaptability, was assessed using several respiratory function parameters. Specifically, "Cchord" is a principal sign of respiratory health in PF, representing the shift in lung compliance throughout recovery. In this study, PNS treatment led to a significant improvement in the values of Cchord, IC, FVC, FRC, and TLC, which were considerably lower in the model group (Fig. 1F).

Subsequently, the levels of α-SMA and transforming growth factor (TGF) β1, both of which are indicators of fibroblast activity, were measured. In the PNS group, a notable reduction was observed in the relative expression levels of α-SMA and TGF β1 mRNA. The expression levels of COL-I and COL-III indicated changes in collagen deposition. Fluorescence labeling was used to measure the expression levels of COL-I, COL-III, and α-SMA in lung tissues. Compared to those in the control group, the concentrations of red fluorescent protein (RFP)-COL-I, green fluorescent protein (GFP)-COL-III, and Cy5-α-SMA were significantly elevated in the model group. However, the fluorescence of RFP-COL-I, GFP-COL-III, and Cy5-α-SMA was quenched upon treatment with PNS (Fig. 1G). Furthermore, treatment with 50, 100, and 200 mg/kg/day PNS reduced the mRNA expression levels of COL-I and COL-III to varying degrees. When the concentrations were compared, the high-dose group showed the most effective results (Fig. 1B). Collectively, these findings suggest that PNS may downregulate both inflammation and collagen deposition in PF therapy.

Autophagy enhancement in mice with PF by PNS

The expression of the autophagy-related protein LC3B II and the LC3 II/LC3 I ratio were significantly increased in the PNS group. Even though the level of the autophagic substrate SQSTM1(P62) was not specified, it decreased markedly in the PNS group (Fig. 2A, B).

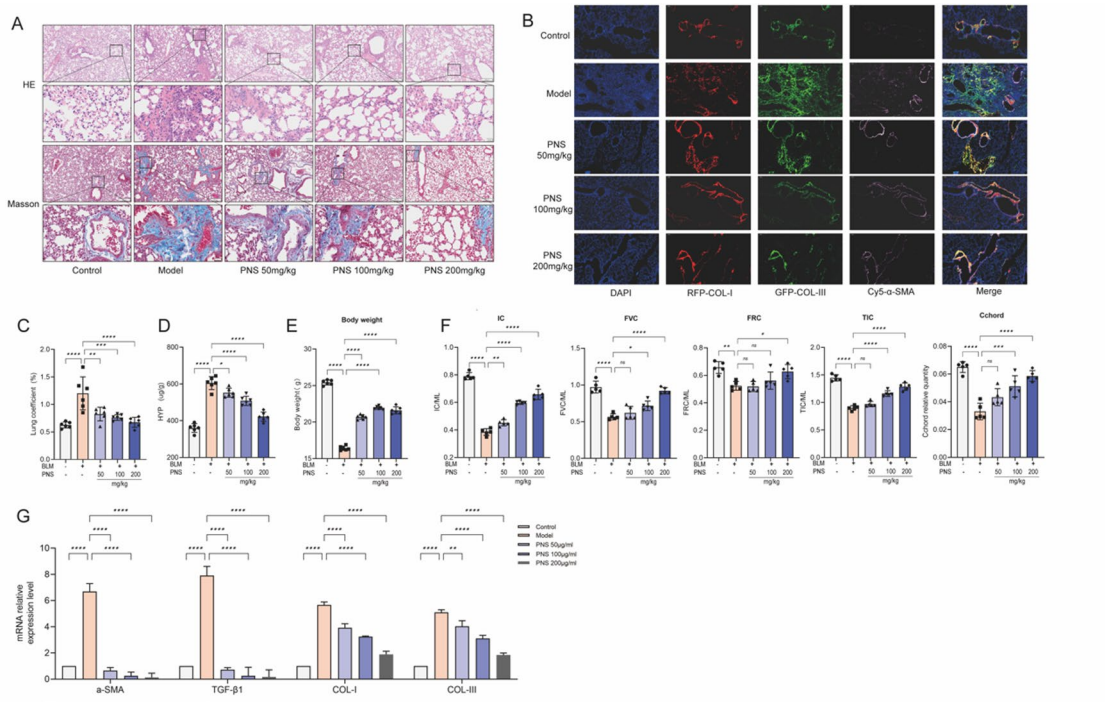

Fig. 1. PNS improves lung damage in mice with PF. **A** Inflammation levels in mice lung tissues were assessed through H&E staining, observed at × 40 and × 200 magnifications, with scale bars measuring 80 μm and 400 μm. Masson staining illustration (magnification: × 40 and × 200, with scale bars of 80 μm and 400 μm). **B** Fluorescent labeling was used to visualize COL-I, COL-III, and α-SMA expression in lung tissue (magnification: × 200, scale bar: 100 μm). **C** Lung coefficient in mice was measured ($n = 6$). **D** Hydroxyproline content in lung tissues, a marker of PF, was quantified ($n = 6$). **E** Final body weight of the mice is shown ($n = 6$). **F** Respiratory function was assessed using an electromedical measurement system($n = 5$). **G** Amounts of α-SMA, TGF-β1, COL-I, and COL-III ($n = 6$).

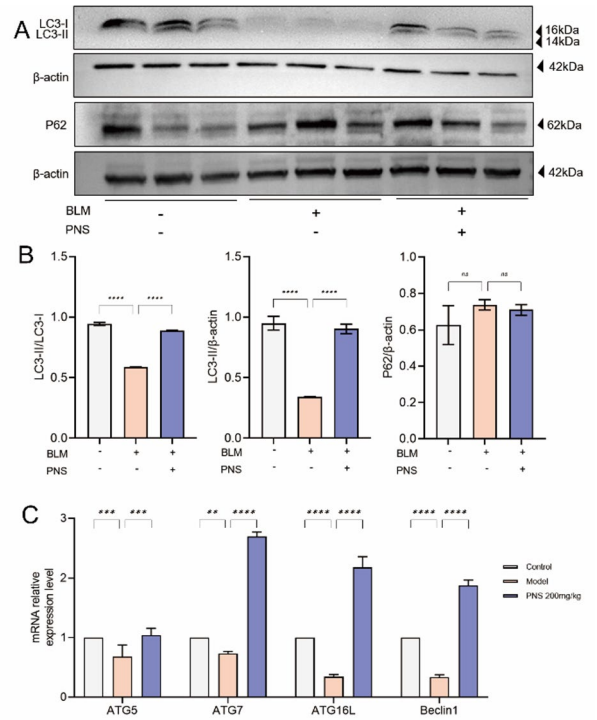

Fig. 2. The administration of PNS induces autophagy in mice with PF. **A**, **B** Levels of LC3-II and P62 expression in the lung tissue of mice. **C** The relative expression degrees of ATG5, ATG7, ATG16L, Beclin 1 mRNA ($n = 3$).

Subsequently, in the PNS group, the levels of ATG5, ATG7, ATG16L, and Beclin 1 were elevated compared to those in the model group (Fig. 2C). These results indicated that PNS was associated with an increase in autophagy in PF.

Lung tissue apoptosis induced by PNS in a PF mice model

In addition to autophagy, apoptosis fulfills a crucial role in PF. In this study, we performed TUNEL staining experiments. In the model group, relatively lower levels of apoptosis were observed within the lung tissue. However, a mass of apoptotic bodies was detected in the PNS group (Fig. 3A). Evaluation of the activities from the Bcl-2 and caspase groups determines the commitment of cells to apoptosis. The expression of the anti-apoptotic protein Bcl-2 was significantly lowered in model mice treated with PNS, whereas the expression of Bax was increased (Fig. 3B, C). Similar results were observed when the Bax and Bcl-2 mRNA levels were measured (Fig. 3D).

It is generally acknowledged that pro-PARP is cleaved upon treatment with PNS. In these experiments, upon PNS treatment, the level of pro-caspase-3 reduced, whereas that of cleaved caspase-3 increased. The model group had lower ratios of cleaved PARP/β actin, cleaved PARP/PARP, cleaved caspase 3/β actin, and cleaved caspase 3/caspase 3 compared to the control group (Fig. 3E, F). Overall, these findings indicated that PNS treatment might significantly induce apoptosis by cleaving PARP and caspase 3.

Reduction of collagen deposition by PNS in HLFs

We performed cell proliferation experiments. The findings confirmed that 25 and 50 μg/mL PNS were suitable for use in subsequent MTS staining cell experiments (Fig. S3). Collagen deposition was observed in HLFs. Using double-labeled immunofluorescence, we observed that TGF β1 stimulation after 12 h led to a substantial rise in COL-I and COL-ΙΙΙ levels. However, upon treatment with PNS, the fluorescence attributable to these was clearly quenched (Fig. 4A). The mRNA levels were also reduced (Fig. 4B). The levels of two fibrosis markers—TGF-β1 and α-SMA—were further reduced upon treatment with PNS. These findings were consistent with those obtained in vivo, suggesting that PNS could mediate therapeutic effects in PF.

ECM elimination depends on autophagy in HLFs

The effects of PNS on autophagy were demonstrated in vivo (Fig. 2). We further explored how autophagy could affect PF in HLFs. First, MDC staining of the PNS group showed the presence of autophagosomes in the cytoplasm (Fig. 5A). Following the successful transfection of MRFP-GFP-LC3 cells, the presence or absence of GFP sequences was verified by agarose gel electrophoresis, in comparison to the control group, which was transfected with an empty plasmid (Fig. S4). An increase in the number of autophagosomes marked with MRFP-GFP-LC3 was observed in the PNS group as opposed to that in the model group (Fig. S5). Moreover, the mRNA expression levels of the autophagy-associated genes *Beclin 1*, *ATG5*, *ATG7*, and *ATG16L* were significantly

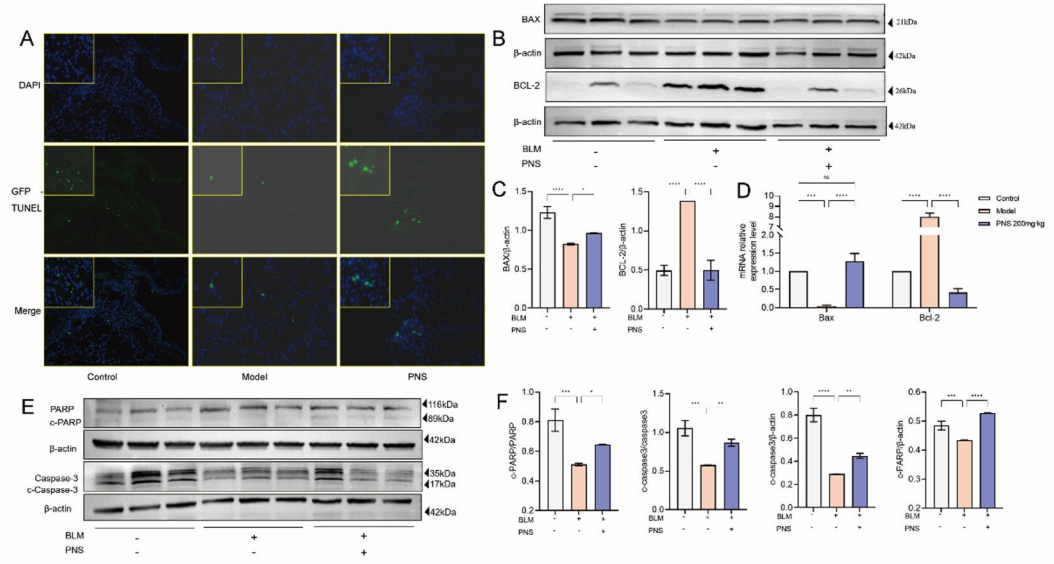

Fig. 3. The administration of PNS resulted in the induction of pulmonary apoptosis in mice with PF. **A** TUNEL stain (magnification, x 200; Scale = 100 μm). **B**, **C** Bax, Bcl2 were detected by WB. **D** Bax, Bcl-2 were detected by qPCR. **E, F** WB was used to detect both PARP and caspase 3, including their cleaved forms. ($n = 3$).

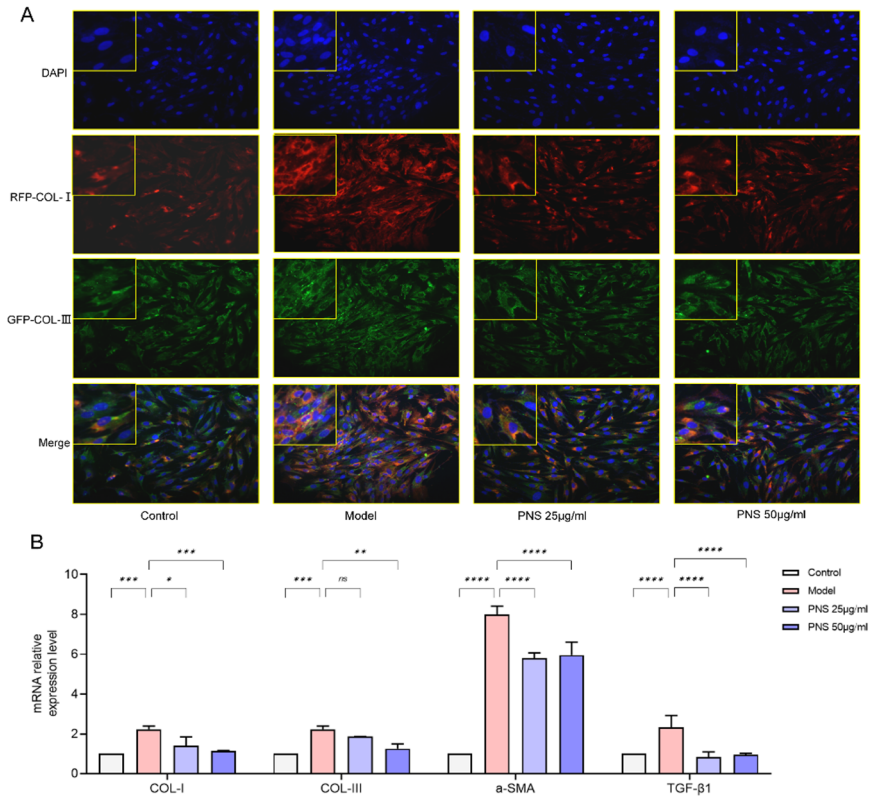

Fig. 4. PNS inhibits collagen deposition in HLFs. **A** Immunofluorescence analysis in COL-I, COL-III (magnification, x 200; scale bar = 120 μm). **B** COL-Ⅰ, COL Ⅲ, TGF β1, as well as α SMA by PCR assay ($n = 3$).

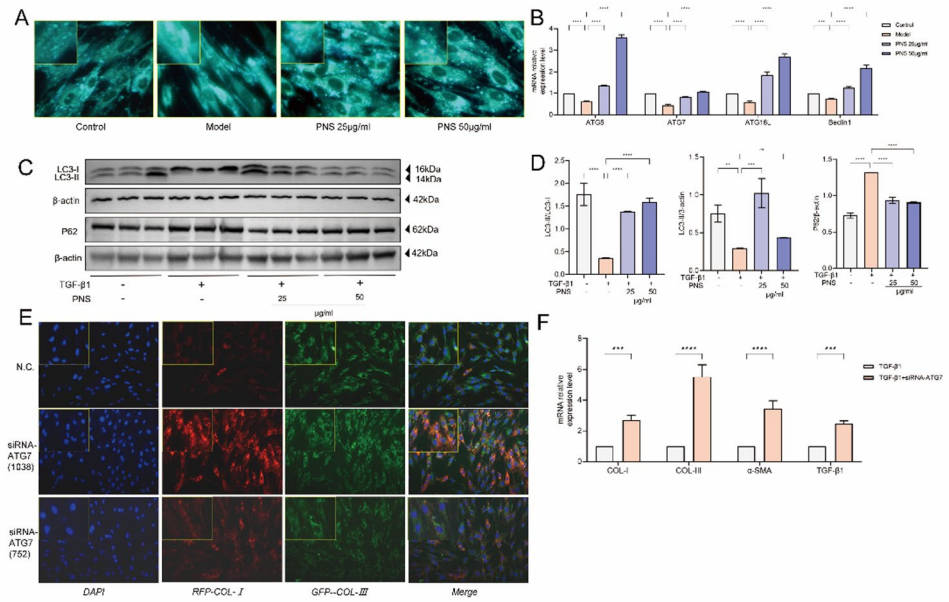

Fig. 5. The elimination of ECM relies on the autophagy process in HLFs. **A** The MDC staining was employed to visualize the autophagosomes. **B** qPCR analysis ATG5, ATG7, ATG16L and Beclin 1 mRNA in HLFs. **C**, **D** LC3B, p62 were detected by WB. **E** After silencing autophagy by siRNA ATG7, the levels of collagen deposition and expression were observed. **F** qPCR analysis α-SMA, COL-I, COL-Ⅲ, along with TGF-β1 in HLFs ($n = 3$).

increased in a dose-dependent manner in the 12 h PNS treatment groups (treated with 25 and 50 μg/mL PNS) (Fig. 5B). Furthermore, compared to that in the model group, the LC3B-II level was increased and P62 level was decreased in the PNS group (Fig. 5C, D).

To assess autophagy function in HLFs, transfection with two siRNA sequences [siRNA-ATG7(1038) and siRNA-ATG7(752)] was performed to suppress the extent of autophagy induced (Fig. S6). The results obtained revealed an increase in the levels of COL-I and collagen fragments (to varying extents) upon treatment with siRNA-ATG7(1038) or siRNA-ATG7(752) (Fig. 5E). Subsequently, the expression of genes associated with collagen deposition, namely *α-SMA*, *COL-I*, *COL-III*, and *TGF β1*, was analyzed. After *ATG7* was knocked down using an siRNA, its mRNA expression levels were found to increase markedly compared to those in the negative control (Fig. 5F).

Activation of apoptosis by PNS contributes to collagen clearance

The function of apoptosis in HLFs was investigated. TUNEL staining experiments were performed to identify apoptotic cells in the PNS group (Fig. 6A). PNS induced the expression of the apoptosis-associated protein Bax. Furthermore, Bax protein activation suppressed the anti-apoptotic gene *Bcl2* (Fig. 6B). Bax and Bcl-2 mRNA expression changed consistently with protein expression. Moreover, the therapeutic effect of PNS was found to be concentration-dependent (Fig. 6C). Compared with that in the model group, the caspase-3 pro-form was cleaved upon treatment with PNS (25 and 50 μg/mL), and an increase in the cleaved form of caspase 3 was observed in the PNS group, with higher ratios of cleaved to non-cleaved caspase 3 and cleaved caspase 3 to β actin observed (Fig. 6D). These results indicated that differences in the extent of apoptosis induced were associated with the therapeutic concentration of PNS. The anti-apoptotic agent Ac-DEVD-CHO was used to block the expression of caspase-3. Fifty micromolar Ac-DEVD-CHO was shown to inhibit apoptosis. The levels of COL-I and COL-Ⅲ changed in accordance with the concentration of Ac-DEVD-CHO added (Fig. 6E). Furthermore, upregulation of modeled mice showed mRNA expression levels for α-SMA, COL-I, COL-Ⅲ, and TGF β1 was observed. When apoptosis was inhibited in HLFs, the mRNA expression levels of the genes increased (Fig. 6F). Therefore, apoptosis activation by PNS aided the remission of collagen accumulation, whereas anti-apoptotic strategies were shown to be detrimental to PF.

Cross-talk between autophagy and apoptosis in HLFs

The results shown in the above experiments collectively suggest that PNS activates autophagy and apoptosis, impairing collagen deposition. We next investigated the association between apoptosis and autophagy in HLFs. After autophagy was disrupted via transfection with siRNA-ATG7, the number of apoptotic cells was found to be reduced (Fig. 7A). The expression of the pro-apoptotic protein Bax was reduced, whereas that of the anti-apoptotic protein Bcl-2 was elevated. Alterations in the mRNA expression levels of both proteins aligned with those in the protein expression levels (Fig. 7B, C). The levels of cleaved PARP and caspase 3 protein were measured. In contrast to that in the control group, the pro forms of caspase 3 and PARP were not cleaved upon

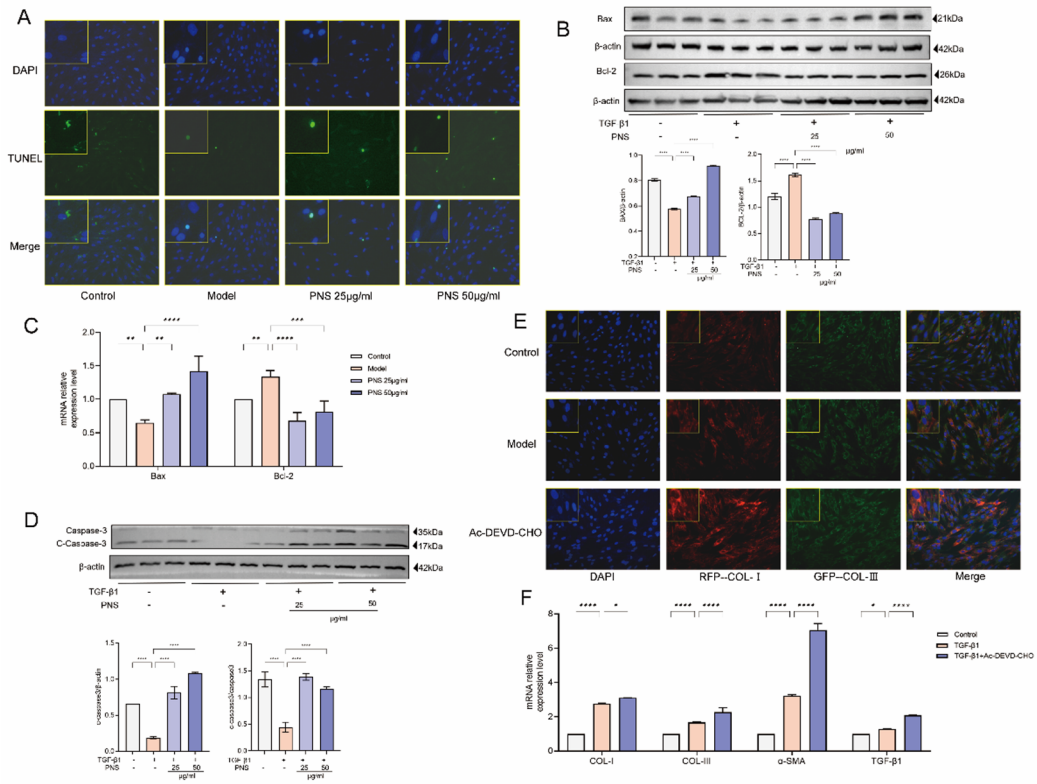

Fig. 6. The activation of apoptosis by PNS contributes to the clearance of collagen. **A** TUNEL staining was performed to assess apoptosis in HLFs. **B** Bax, Bcl-2 proteins were measured by WB. **C** qPCR analysis was conducted to determine the mRNA expression of Bax and Bcl-2 in HLFs. **D** WB was used to detect caspase-3 and c-caspase-3. **E** Autophagic bodies were stained post-treatment with the AC-DEVD-CHO. **F** qPCR regease α-SMA, COL-I, COL-ⅢI, TGF-β1 after AC-DEVD-CHO inhibitor intervention ($n = 3$).

autophagy impairment in HLFs (Fig. 7D). These findings collectively indicate that autophagy is a key component in the signaling pathway that regulates apoptosis in HLFs.

We investigated whether changes in the extent of apoptosis were associated with fluctuations in the level of autophagy. Apoptosis was inhibited using the inhibitor Ac-DEVD-CHO, and changes in autophagy in HLFs were subsequently observed. MDC staining experiments revealed that the autophagosomes did not show any significant differences (Fig. 7F). The number of autophagosomes did not change significantly in the Ac-DEVD-CHO-treatment group (Fig. S7). Moreover, the LC3-II and P62 levels did not change significantly upon apoptosis inhibition (Fig. 7E). Compared to that in the model group, the expression of the autophagic gene cluster, including *ATG5*, *ATG7*, *ATG16L*, and *Beclin-1*, did not show significant differences following Ac-DEVD-CHO treatment (Fig. 7G). Collectively, these findings suggested that while autophagy is not dependent on fluctuations in apoptosis, apoptosis is dependent on autophagy in HLFs.

PI3K/AKT pathway suppression by PNS in PF

Using network pharmacological analysis and based on experimental evidence, we outlined how PNS regulates the PI3K/AKT pathway in relation to PF. Insights from network pharmacology analysis showed that a complex interrelation among PNS, PF, and the PI3K/AKT pathway is a prominent target for intervention, owing to its connection to autophagy and apoptosis (Figs. S8, S9). Studies conducted in animal and cell models revealed a significant increase in the PI3K/AKT protein levels in PF models, which reduced considerably upon treatment with PNS (Fig. 8A–D). The use of AKT inhibitors (MK-2206 dihydrochloride, 10 mM/mL, MedChemExpress LLC, cat.no. HY-10358) effectively inhibited the downstream effects of this signaling pathway, further supporting our observations. The results of in vitro experiments demonstrated that AKT inhibition amplified the expression of proteins involved in autophagy and apoptosis (Fig. 8E–G). Collectively, these findings articulate the therapeutic potential of PNS, which appears to attenuate PF by suppressing the PI3K/AKT signaling pathway and enhancing apoptosis and autophagy, thereby enriching the therapeutic landscape for PF management.

Molecular targets interacting with PNS in PF

Initially, we used network pharmacology to identify 67 shared potential targets of action. Subsequently, we corroborated the feasibility of using these targets through molecular docking techniques, which helped identify the top 15 targets demonstrating high binding affinity (Fig. S10). To evaluate the interaction potential between these key PNS components and core targets, we conducted binding score-based screening. Among the components,

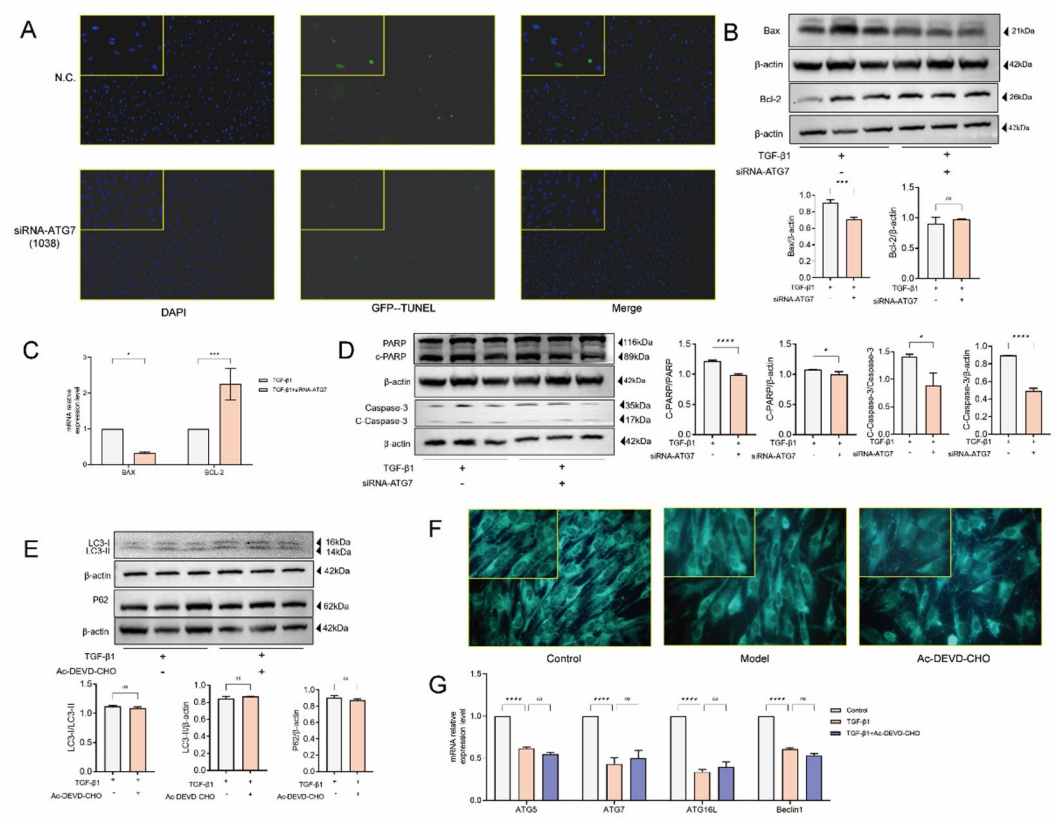

Fig. 7. Autophagy cross talk with apoptosis in HLFs. **A** TUNEL staining of HLFs is shown. **B** HLFs were transfected with 50 nm ATG7-siRNA, Bax, Bcl-2 expression was detected by WB. **C** After ATG7 silencing, Bcl-2, Bax mRNA levels in HLFs were analyzed by qPCR. **D** WB was applied to discover PARP, its cleaved form, caspase 3, and its cleaved form. **E** Following AC-DEVD-CHO inhibitor treatment, WB was used to detect LC3-II, p62 expression in HLFs. **F** MDC staining for autophagosomes is shown. **G** After AC-DEVD-CHO treatment, qPCR was used to assess ATG5, ATG7, ATG16L, and Beclin 1 mRNA levels in HLFs ($n = 3$).

ginsenoside-Rh1 exhibited the highest predicted binding affinity for the corresponding targets illustrated in the figure, which was consequently selected to visualize the molecular binding conformation depicted in Fig. 9A. Eight candidates with the highest score were identified. The mRNA expression of *HSP90AA1*, *KDR*, *MAPK1*, *STAT3*, *EGFR*, *ESR1*, *GRB2*, and *HIF1A* was assessed. The expression of these genes increased in the model group compared to that in the control. Interestingly, when apoptosis, autophagy, and AKT expression were inhibited, the expression levels of these biomarkers showed different alterations (Fig. 9). Apoptosis inhibition led to altered expression of *HSP90AA1*, *KDR*, *MAPK1*, *STAT3*, *ESR1*, *GRB2*, and *HIF1A*. Autophagy inhibition led to the elevation of *HSP90AA1* and *EGFR* expression and disruption of AKT expression. This reduced the transcription levels of *HSP90AA1*, *KDR*, *MAPK1*, *STAT3*, *EGFR*, *ESR1*, *GRB2*, and *HIF1A*. Therefore, the modulation of apoptosis, autophagy, and PI3K/AKT pathways could affect the expression profiles of molecular targets that are associated with the action and efficacy of PNS.

Discussion

A range of chemical, physical, and biological factors leads to PF. Persistent alveolar damage, repair and reconstruction, fibroblast proliferation, and excessive interstitial fibrous connective tissue deposition in the alveoli are some of the processes that induce PF[33]. The treatment methods approved for PF are associated with substantial adverse side effects, which considerably impact the quality of life of patients. Currently, PF treatment with nintedanib and pirfenidone has been approved by the U.S. FDA. This therapy can cause diarrhea, nausea, and other side effects[3]. This necessitates the identification of new therapeutic candidates with less severe adverse effects. Saponins, including R_1, Rg_1, and Rb_1, are the primary constituents of *P. notoginseng*. The non-saponin compounds in this ethnomedicine primarily include polysaccharides, flavonoids, and amino acids[34]. PNS is the primary active ingredient in *P. notoginseng*. Previous research has demonstrated that treatment with *P. notoginseng* markedly increases cell viability and enhances superoxide dismutase and catalase activities within cells, while reducing the levels of reactive oxygen species and malondialdehyde[35,36]. Additional effects associated with PNS treatment have now been identified. Animals with PF treated with PNS showed a significant lowering of the rate of inflammatory cell infiltration and collagen fiber deposition. Notably, following treatment with PNS, the levels of hydroxyproline and several fibrosis-inducing factors, α SMA, TGF β1, COL-I, and COL-III were

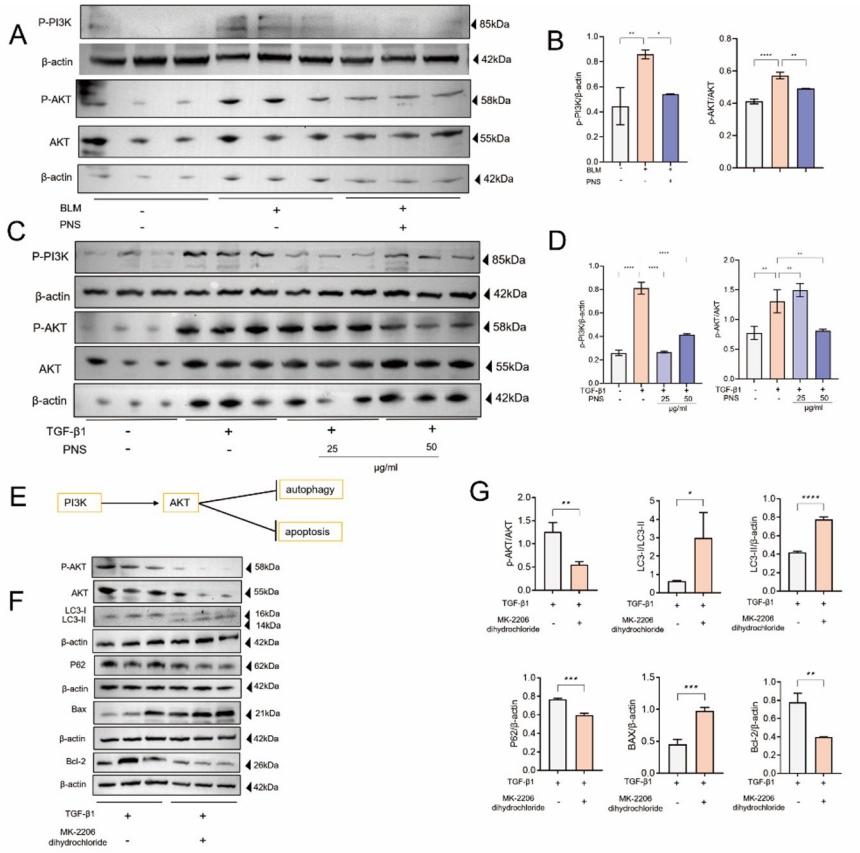

Fig. 8. PNS inhibited the PI3K/AKT signaling route in PF. **A**, **B** Signaling route proteins in mice lung tissues were analyzed by WB. **C**, **D** These proteins in HLFs were also assessed by WB. **E** The PI3K/AKT pathway regulates apoptosis and autophagy. **F**, **G** Following MK-2206 dihydrochloride treatment, WB measured apoptosis- and autophagy-related proteins in HLFs ($n = 3$).

considerably lowered. The lung damage caused by inflammation was also ameliorated, indicating the potential anti-fibrotic properties of PNS in PF.

Subsequently, the mechanism(s) underlying the involvement of PNS in autophagy and apoptosis were explored. Autophagy is an evolutionarily preserved homeostatic mechanism that affects the degradation pathway mediated by lysosomes, contributing to the recycling of organelles and proteins[37]. As a process, autophagy is beneficial for alleviating PF and multifactorial pulmonary fibrotic diseases, including cystic fibrotic lung disease, smoking-induced PF, idiopathic PF, and ionizing radiation-mediated PF[38]. Autophagy maintains homeostasis in lung fibroblasts and is an attractive target in anti-PF therapies. Autophagy inhibition has been found to regulate fibroblast differentiation into myofibroblasts, a pulmonary process that is associated with fibrosis[39]. Impairments in autophagy enhance TGF β1 and increase ECM accumulation. LC3-II protein expression was found to be reduced in the lung tissues of individuals with PF and autophagy[40]. Two ubiquitin-like conjugation systems, the ATG5/ATG16L/ATG7 system and the LC3 system, are essential for the elongation and maturation of autophagosomes. This research also demonstrated that Beclin 1 and LC3-II levels were notably decreased in the PF mice model. Only autophagosomes were observed under an electron microscope. In particular, upon treatment with PNS, the number of autophagosomes increased, and the gene cluster associated with autophagy, including *LC3II*, *ATG5*, *ATG16L*, *ATG7*, and *Beclin 1*, was upregulated, whereas the substrate p62 was found to be consumed. These findings suggest that PNS can activate autophagy in PF. The concentrations of COL-I, COL-III, TGF β1, and α SMA were markedly upregulated upon the knockdown of the autophagy-associated gene *ATG7*. Collectively, these findings support the fact that autophagy is necessary to reduce collagen deposition and indicate that autophagy inhibition increases collagen deposition.

Apoptosis is a metabolically active process for cell death, characterized by distinct morphological changes, including cell membrane contraction, nuclear chromatin condensation, and the nuclear removal of debris[41]. The regulation of cell death is critical for organisms. The lungs should maintain a delicate epithelial-endothelial interface network that allows efficient carbon dioxide and oxygen exchange[42]. Apoptosis can occur owing to the deactivation of growth factors, oxidative stress, endoplasmic reticulum stress, and DNA damage in lung tissues. A previous study demonstrated that apoptosis is markedly inhibited in PF[43]. PNS therapy was found to be associated with a mass of apoptotic bodies. The cleavage of pro-PARP and pro-caspase-3, accompanied by an increase in the level of Bax protein, suggested that PNS prevents PF by promoting apoptosis via the cleavage of PARP and caspase-3. A former clinical study showed that the presence of a large number of fibroblastic foci

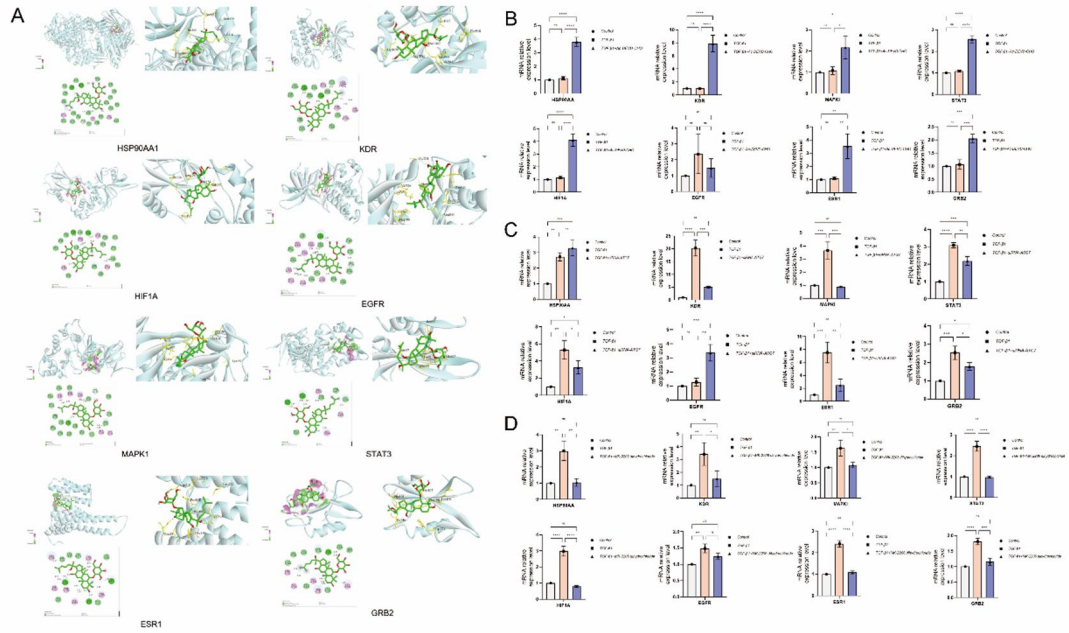

Fig. 9. Molecular targets interacting with the PNS in PF. **A** Visual analysis of molecular docking of HSP90AA1, KDR, MAPK1, STAT3, EGFR, ESR1, GRB2, and HIF1A. **B**–**D** After AC-DEVD-CHO intervention, after silencing autophagy by siRNA ATG7, and MK-2206 dihydrochloride intervention, the mRNA transcription levels of HSP90AA1, KDR, MAPK1, STAT3, EGFR, ESR1, GRB2, and HIF1A of n human lung fibroblast ($n = 3$).

in lung biopsies was associated with higher mortality in patients with PF[44]. Therefore, the dynamic process of apoptosis may explain, in part, the therapeutic effects of PNS according to its self-destructive processes, also providing a focal point for the development of targeted therapies against PF.

Autophagy and apoptosis are two mechanisms of cellular destruction that help preserve homeostasis. It has been suggested that there is a communication between these processes[45]. In specific situations, autophagy serves as a mechanism for stress adaptation that inhibits apoptosis, helping prevent cell death. However, in different cellular contexts, autophagy can also provide a distinct pathway leading to cell death[46]. Autophagy not only inhibits the activation of caspase 3, which is linked to apoptosis, thus preventing its induction and minimizing cellular damage, but can also, depending on the conditions, trigger apoptosis[47]. In this study, the impairment of autophagy occurred in conjunction with the suppression of apoptosis-related genes and proteins. Autophagy may be an upstream signal that influences apoptosis in PF. Hepatic apoptosis has previously been shown to be regulated by autophagic activity[48]. Autophagy regulates apoptosis and cell growth and differentiation in acute lymphoblastic leukemia[49,50]. The balance among these processes is regulated by the AMPK, PI3K/Akt/GSK3β, and p38/JNK/MAPK routes[50]. Upon apoptosis inhibition, the expression levels of autophagy-related genes and proteins remained unaffected, supporting the fact that autophagy operates independently of apoptosis in cells. Therefore, PNS might trigger crucial multi-target self-destructive processes (both autophagy and apoptosis) to reduce inflammation and ECM deposition, which are beneficial for alleviating lung damage in PF.

Our research describes the molecular processes of autophagy and apoptosis in PF pathophysiology. Both processes play crucial roles in the therapeutic effects of PNS in PF, particularly in activating autophagy and apoptosis to reduce extracellular collagen deposition. In addition, conceptual evidence has been provided to show that the activation of autophagy and apoptosis by PNS may be used to treat progressive fibrotic diseases. PNS exerts multi-target, anti-PF effects, which provide a novel approach for PF prevention and treatment. We believe our findings will lead to further research on the impact of PNS on autophagy and apoptosis within PF, confirming that these pathways are potential therapeutic targets.

Network pharmacology analysis and experimental validation have highlighted the essential function of the PI3K/AKT pathway in PF, suggesting that PNS may target this pathway, which is enriched in autophagic and apoptotic processes within the pathophysiological milieu of PF. Our results from in vivo and in vitro experiments corroborate this hypothesis, as indicated by an upregulation of PI3K/AKT pathway proteins in the PF model, which was attenuated upon PNS administration. These findings are consistent with previous research findings that underscore the significance of the PI3K/AKT pathway in various fibrotic diseases and its potential as a therapeutic target[51,52]. The diminished expression of PI3K/AKT pathway proteins following PNS treatment indicates that PNS may exert its therapeutic effects by modulating this signaling cascade. Our research focused on these findings, showing that when AKT activity is inhibited, the downstream processes of autophagy and apoptosis are enhanced, as evidenced by the increased expression of autophagy- and apoptosis-related proteins in HLFs treated with AKT inhibitors. This confirmed the pathway's interplay with cellular survival mechanisms. Moreover, using network pharmacology and molecular docking, we identified eight targets—HSP90AA1,

	Name	MS1 ppm	Electric	Mzmed	Rtmed
①	Ginsenoside Rh1; GinsenosideF1; Sanchinoside B1;	− 2.16715953870515; − 2.16715953870515; − 2.16715953870515;	+H	603.4247917	118.285
②	Ginsenoside Rh1; Ginsenoside F1; Sanchinoside B1;	− 2.16715953870515; − 2.16715953870515; − 2.16715953870515;	+H	621.4342238	118.285
③	3− Galloylgallocatechin; Epigallocatechin gallate; Soyasapogenol B; Soyasapogenol F;	5.01776178600889; 5.01776178600889; − 4.36323018646855; − 4.36323018646855	+H	441.3714503	117.0055
④	Ginsenoside Rh1; Ginsenoside F1; Sanchinoside B1;	− 3.73347895079656; − 3.73347895079656; − 3.73347895079656;	−H	697.4523562	120.742
⑤	Ginsenoside A2; Ginsenoside Ia; Ginsenoside Rf; Ginsenoside A1; Ginsenoside Rg1;	− 1.5078222991647; − 1.5078222991647; − 1.5078222991647; − 1.5078222991647; − 1.49907769249948;	−H	859.5038997	217.776
⑥	Ginsenoside Rg3; Ginsenoside F2; Ginsenoside C; Gypenoside LXXV; Ginsenoside LXXV;	− 2.92212608277389; − 2.92212608277389; − 2.92212608277389; − 2.93181378698319; − 2.93181378698319;	−H	843.5100001	180.658
⑦	Ginsenoside F5; Notoginsenoside R2; Pseudoginsenoside RT3; Ginsenoside F3;	− 2.13152385442329; − 2.13152385442329; − 2.13152385442329; − 2.13152385442329;	−H	769.4736289	187.518
⑧	Ginsenoside Rh1; Ginsenoside F1; Sanchinoside B1;	− 3.73347895079656; − 3.73347895079656; − 3.73347895079656;	−H	637.4299726	120.102
⑨	Notoginsenoside R1; Cyclofoetoside B; Notoginsenoside R1	0.572847459840561; 0.536173192507276; 0.536173192507276	−H	991.546578	260.813

Table 1. The primary active ingredient in the total saponins of *Panax notoginseng*. Mzmed: Median mass-to-charge ratio, representing the mass-to-charge ratio of this peak across all samples. Rtmed: Median retention time, representing the retention time of this peak across all samples. Electric: Indicates the charge property of the detected substance (positive charge or negative charge).

KDR, MAPK1, STAT3, EGFR, ESR1, GRB2, and HIF1A—which exhibited high-affinity interactions with PNS components. These targets were verified in HLFs and may be critical nodes within the PI3K/AKT pathway to modulate the processes in PF.

Overall, the results of this study have shown that PNS may be used to treat PF to trigger the degradation of collagen deposits. Mechanistically, the efficacy of PNS is related to autophagy and apoptosis. Further investigation revealed that PF development may also be influenced by the PI3K/AKT pathway.

Method and materials

Plant material

The main ingredient of. *P. notoginseng, Panax notoginseng* saponins (PNS), was sourced from Beijing Solarbio Science & Technology Co., Ltd. in Beijing, China (cat.No.S4820).With PNS as the main active constituent, UHPLC-QTOF-MS was then carried out to identify active the ingredients. The PNS fingerprint revealed 41 peaks, and the primary peaks were clearly separated (Fig. S1). Upon further analysis, the main nine peaks were identified as *ginsenoside*, *notoginsenoside*, *epigallocatechin gallate*, *soyasapogenol*, *cyclofoetoside*, *gypenoside*, *sanchinoside*, *pseudoginsenoside* and other components (Table 1 and Fig. S2). The active product may be one or more of these ingredients.

Animals and treatment

SPF (Beijing) Biotechnology Co., Ltd. supplied thirty male Kunming (KM) mice, aged between 6 and 8 weeks. Except for the control group, the BLM-treated mice (Zhejiang Hisun Pharmaceutical Co., Ltd.) were allocated to groups at random (n = 6 for each group), including the model and drug intervention groups with three different concentrations. To create the BLM-induced pulmonary fibrosis model, the following procedure was used: after anesthetizing the mice with intraperitoneal sodium pentobarbital (50 mg/kg), A tracheal injection was used to administer BLM at a dose of 5 mg/kg, an equivalent volume of normal saline was administered to the control group. Seven days later, we started administering PNS treatment. Corresponding to the model group, the PNS group of mice were administered 50, 100, 200 mg/kg/day PNS via gavage, the same volume of carrier was administered to both the control and model groups[53,54]. As recommended in the American Veterinary Medical Association's Animal Euthanasia Guidelines (2020), pentobarbital sodium (200 mg/kg) was injected intraperitoneally to perform euthanasia on the 28th day. Blood was rapidly collected from the abdominal aorta, the lung tissue was collected, and the body was otherwise disposed of according to the recommended guidelines. Cessation of the life functions of the mice was deemed to have occurred when they had neither a heartbeat nor any nerve reflexes.

Ethics approval

All experiments involving mice received approval from the Animal Ethical Experimentation Committee at Yunnan University of Chinese Medicine and all experiments were conducted in accordance with their relevant guidelines and regulations (no. R 062023073). According to the Guide for the Care and Use of Laboratory Animals, the principles of replacement, reduction, and refinement are crucial, were followed to minimize animal distress, including the elimination of drug serum testing and using the minimum number of animals for statistical analysis. The study was conducted in accordance with the ARRIVE guidelines.

Cells culture

Human lung fibroblasts (HLFs, KCB 200695) were sourced from the Conservation Genetics CAS Kunming Cell Bank in Kunming, China and were grown in DMEM (C11965500BT, Gibco, USA) combined with 10% FBS (10091148, Gibco, USA) with 1% penicillin and streptomycin (P1400, Solarbio, China) at 37 °C in a 5% CO2 surroundings. The cells were subjected to 10 ng/mL of TGF-β1 once they achieved 50–60% confluence (Beijing

Solarbio Science & Technology Co., Ltd.) for 12 h. Subsequently, HLFs were treated with 25 and 50 μg/mL PNS for 12 h.

Lung coefficient analysis

After 28 days of PNS treatment, the mice were (in g) weighed and anesthetized before being sacrificed as described previously. Lung tissue was quickly collected, and the wet lung weight in milligrams was recorded, and the lung coefficient was calculated as (wet lung weight in mg / body weight in g) multiplied by 100%.

Evaluation of respiratory function as measured via an electro-medical measurement system

To anesthetize the mice, pentobarbital sodium was given intraperitoneally at 50 mg/kg, and their tracheas were fully exposed and opened prior to the intubation of a dedicated tracheal tube into the trachea. The Electro-Medical Measurement System Division of Information (Display Systems Ltd.) was subsequently utilized to assess the lung function measurements in mice.

H&E staining

The lungs of the mice were removed, fixed in 4% paraformaldehyde for 24 h, dehydrated using a series of ethanol solutions, embedded in paraffin, and then examined under a light microscope following H&E staining.

Masson staining

Mice lung tissue was preserved in 4% paraformaldehyde and prepared for paraffin embedding. The sections were incubated in xylene (2 × 20 min), absolute ethanol, and 75% ethanol, followed by water washing. The tissue was then soaked in potassium dichromate overnight, washed with distilled water, and stained sequentially with hematoxylin iron), ponceau red acid magenta dye, phosphomolybdic acid, aniline blue solution, and 1% glacial acetic acid. Ultimately, the sections underwent dehydration in absolute ethanol, were cleared in xylene, and mounted using neutral gum.

Fluorescence triple labeling

Lung tissue sections were incubated with antibodies: anti-collagen I (1:500; catalog number ab138492; Abcam), anti-collagen III (1:500; catalog number ab7778; Abcam), or anti-α smooth muscle actin. The sections were subsequently incubated with fluorescent secondary antibodies: 488 goat anti-rabbit (1:400; catalog number GB25303) and Cy3 goat anti-rabbit (1:300; catalog number GB21303). The slices were washed, mounted with a medium that prevents fluorescence quenching, and then observed under a fluorescence microscope for imaging after adding an autofluorescence quencher.

Immunofluorescence experiments

Prepare cell slides and post-fixation. The cells were subsequently incubated with primary antibodies targeting COL-I and COL-III, followed by fluorescent secondary antibodies, 488 goat anti-rabbit (1:1,000; cat. no. GB25303; Wuhan Servicebio Technology Co., Ltd.) and Cy3 goat anti-rabbit (1:1,000; cat. no. GB21303; Manufacturer ibid.), were applied. Finally, the images were captured after observing the slides with a fluorescence microscope.

TUNEL staining

Mice lung tissues were sectioned and dehydrated through xylene and ethanol series. The tissues were treated with proteinase K at 37 °C, washed using PBS and then incubated in a solution that digests tissue. After PBS washing, the TUNEL reaction mixture (TdT and dUTP) was applied and incubated at 37 °C. After additional PBS washes, DAPI staining was applied, and the slides were mounted with anti-fluorescence quenching medium. The same TUNEL protocol was used for cells.

Monodansylcadaverine (MDC) staining observation of autophagosomes

HLFs were digested with 0.25% trypsin, centrifuged at 500 g for 5 min, and washed with 1X Wash buffer. The cell suspension was aliquoted (90 μl) into a new tube, and MDC stain (10 μl) was added, followed by gentle mixing. The cells were stained in the dark for a time span of 15 to 45 min, then centrifuged at 500 g for 5 min. After two washes with 1X Wash buffer, the liquid portion was discarded, and collection buffer (100 μl) was added and mixed. Ultimately, the cells were examined and imaged using a fluorescence microscope with an excitation filter of 355 nm and a blocking filter of 512 nm.

Hydroxyproline assay

Fresh lung tissue was weighed as per the manufacturer's guidelines (A030-2-1, Nanjing Jiancheng Bioengineering Institute), the supernatant was obtained after a series of chemical reactions, and subsequently the optical density (OD) value was evaluated using enzyme-labeled apparatus (SYNERGY H1,BIO-RAD Co., Ltd.). The findings were presented as micrograms of hydroxyproline per gram of wet lung weight (μg/g).

qPCR assay

Mice lung tissue and HLFs were used to extract total RNA for cDNA synthesis. The qPCR experiment was performed according to the instructions. Primer sequences for PCR are listed in Supplementary material Tables 1 and Supplementary material Table 2.

Western blot assay

Total proteins were obtained from the lung tissues of mice and HLFs. A BCA protein assay served as a means to calculate the total protein concentration. SDS polyacrylamide gels were used to separate the total protein

lysate (40 μg) in each well, and use PVDF membrane (cat no. IPVH00010; MilliporeSigma), to detect protein expression. The main antibodies utilized included the Anti LC3B rabbit polyclonal antibody at a 1:1,000 dilution (catalog number L7543; Sigma Aldrich), anti-SQSTM1/P62 rabbit polyclonal antibody (1:1,000; P0067; Sigma-Aldrich), anti-PARP rabbit monoclonal antibody (1:1,000; ab191217; Abcam), anti-caspase-3 rabbit monoclonal antibody (1:1,000; ab184787; Abcam), rabbit-derived polyclonal antibody for Bax (1:1,000; 50599-2-Ig; Proteintech Group, Inc.), anti-Bcl-2 rabbit polyclonal antibody (1:1,000; 26593-1-AP; Proteintech Group, Inc.), Phospho-PI3K p85 alpha (Tyr607) Ab (1: 500; cat. no. AF3241; Affinity Biosciences), Phospho-AKT (Ser473) Recombinant antibody (1:5,000; cat. no. 80455-1-RR; Proteintech Group, Inc.), AKT Polyclonal antibody (dilution 1:2,000; catalog number 10176-2-AP; Proteintech Group, Inc.) and anti β actin mouse monoclonal antibody (dilution 1:5,000; catalog number 60008 1 Ig; Proteintech Group, Inc.).

RNA interference assay

ATG7-siRNA (Shanghai GenePharma Co., Ltd.) was used at a concentration of 60–70% in Invitrogen® Opti-MEM medium with Invitrogen® Lipofectamine 2000™ transfection agent (Thermo Fisher Scientific, Inc.), according to the instructions provided by the manufacturer, the control group had its negative control replaced 12 h after transfection, and the gene silencing efficiency was assessed by qPCR. The following siRNAs were used: ATG7-mus-752, forward sequence: GGAGCAUGCCUAUGAUGAUTT, and reverse sequence: AUCAUCAUA GGCAUGCUCCTT; and ATG7-mus-1038, forward sequence: GCUAGAGACGUGACACAUATT, and reverse sequence: UAUGUGUCACGUCUCUAGCTT.

Transfection of MRFP-GFP-LC3 plasmid

MRFP-GFP-LC3 plasmid (kindly donated by Professor Zou Jiaqing of Yunnan University, Kunming, China) was transfected into HLFs for autophagy detection when the density of the transfected cells accounted for approx. 80% of the culture plate, and the cells were treated with PNS (25ug/ml and 50 ug/ml,24 h). Microscopic observation (Nikon DS-FIIC; Nikon Corporation). The GFP sequences used for fluorescence tagging are: EGFP-N: CGTCG CCGTCCAGCTCGACCAG; EGFP-C: CATGGTCCTGCTGGAGTTCGTG.

Network Pharmacological analysis and molecular docking verification

Utilizing network pharmacology, we meticulously analyzed the drug component targets of *Panax notoginseng* saponins (PNS), the disease-modulatory targets of PF, and the pivotal targets involved in autophagy and apoptosis. This comprehensive analysis facilitated the identification of principal target proteins, which were subsequently subjected to rigorous validation through molecular docking. We have focused on the PI3K-AKT signaling pathway[55], for an in-depth exposition of the data and the nuanced methodological approaches employed, readers are directed to Supplementary material 1, which contains elaborate details.

Statistical analysis

All experiments were randomized and conducted in a blinded fashion. Group randomization was used to randomize the samples, i.e., the KM mice and HLFs, into groups of a specified sample size. No KM mice or HLFs were excluded from the analysis. The data are shown as the mean ± SEM, and statistical significance was assessed using one-way ANOVA with Tukey's post-hoc test for multiple comparisons. The p value less than 0.05 was deemed significant, with ns indicating not significant; $^{*}P<0.05$; $^{**}P<0.01$; $^{***}P<0.001$; $^{****}P<0.0001$. The p value is no longer represented in the legend of the result below.

Data availability

To access the datasets utilized and/or examined in this research, please contact the corresponding author with a reasonable request.

Received: 1 March 2025; Accepted: 4 November 2025
Published online: 27 November 2025

References

1. Wijsenbeek, M. Progress in the treatment of pulmonary fibrosis. *Lancet Respir. Med.* **8** (5), 424–425 (2020).
2. Shenderov, K., Collins, S. L., Powell, J. D. & Horton, M. R. Immune dysregulation as a driver of idiopathic pulmonary fibrosis. *J. Clin. Investig.* **131** (2), e143226 (2021).
3. Spagnolo, P. et al. Idiopathic pulmonary fibrosis: disease mechanisms and drug development. *Pharmacol. Ther.* **222**, 107798 (2021).
4. Habermann, A. C. et al. Single-cell RNA sequencing reveals profibrotic roles of distinct epithelial and mesenchymal lineages in pulmonary fibrosis. *Sci. Adv.* **6** (28), eaba1972 (2020).
5. Lv, X., Li, K. & Hu, Z. Autophagy and pulmonary fibrosis. *Adv. Exp. Med. Biol.* **1207**, 569–579 (2020).
6. Chillappagari, S. et al. Therapeutic induction of Bcl2-associated athanogene 3-mediated autophagy in idiopathic pulmonary fibrosis. *Clin. Transl. Med.* **12** (7), e935 (2022).
7. Katzen, J. & Beers, M. F. Contributions of alveolar epithelial cell quality control to pulmonary fibrosis. *J. Clin. Investig.* **130** (10), 5088–5099 (2020).
8. Kitada, M. & Koya, D. Autophagy in metabolic disease and ageing. *Nat. Rev. Endocrinol.* **17** (11), 647–661 (2021).
9. Galluzzi, L. & Green, D. R. Autophagy-independent functions of the autophagy machinery. *Cell* **177** (7), 1682–1699 (2019).
10. Sosulski, M. L. et al. Deregulation of selective autophagy during aging and pulmonary fibrosis: the role of TGFβ1. *Aging Cell* **14** (5), 774–783 (2015).
11. Divya, T., Sureshkumar, A. & Sudhandiran, G. Autophagy induction by celastrol augments protection against bleomycin-induced experimental pulmonary fibrosis in rats: role of adaptor protein p62/ SQSTM1. *Pulm Pharmacol. Ther.* **45**, 47–61 (2017).
12. Rangarajan, S. et al. Novel mechanisms for the antifibrotic action of nintedanib. *Am. J. Respir Cell. Mol. Biol.* **54** (1), 51–59 (2016).
13. He, J. et al. Isoliquiritigenin inhibits TGF-β1-induced fibrogenesis through activating autophagy via PI3K/AKT/mTOR pathway in MRC-5 cells. *Acta Biochim. Biophys. Sin (Shanghai)* **52** (8), 810–820 (2020).

14. Hinz, B. & Lagares, D. Evasion of apoptosis by myofibroblasts: a hallmark of fibrotic diseases. *Nat. Rev. Rheumatol.* **16** (1), 11–31 (2020).
15. Carneiro, B. A. & El-Deiry, W. S. Targeting apoptosis in cancer therapy. *Nat. Rev. Clin. Oncol.* **17** (7), 395–417 (2020).
16. Kuo, W. T. et al. Inflammation-induced occludin downregulation limits epithelial apoptosis by suppressing Caspase-3 expression. *Gastroenterology* **157** (5), 1323–1337 (2019).
17. Rangarajan, S. et al. Metformin reverses established lung fibrosis in a bleomycin model. *Nat. Med.* **24** (8), 1121–1127 (2018).
18. Ricci, A. et al. Decreased expression of autophagic Beclin 1 protein in idiopathic pulmonary fibrosis fibroblasts. *J. Cell. Physiol.* **228** (7), 1516–1524 (2013).
19. Zhan, P. et al. Assessment of suitable cultivation region for *Panax notoginseng* under different Climatic conditions using maxent model and high-performance liquid chromatography in China. *Ind. Crops Prod.* **176**, 114416 (2022).
20. Hu, D. et al. Sanqi oral solution ameliorates renal fibrosis by suppressing fibroblast activation via HIF-1α/PKM2/glycolysis pathway in chronic kidney disease. *J. Ethnopharmacol.* **335**, 118679 (2024).
21. Yang, F. et al. Screening of active components in astragalus mongholicus bunge and *Panax notoginseng* formula for anti-fibrosis in CKD: nobiletin inhibits Lgals1/PI3K/AKT signaling to improve renal fibrosis. *Ren. Fail.* **46** (2), 2375033 (2024).
22. Han, J. et al. Using network Pharmacology to explore the mechanism of *Panax notoginseng* in the treatment of myocardial fibrosis. *J. Diabetes Res.* **2022** (1), 8895950 (2022).
23. Xu, C. et al. Analytical methods and biological activities of *Panax notoginseng* saponins: recent trends. *J. Ethnopharmacol.* **236**, 443–465 (2019).
24. Liu, M. et al. Preparation, optimization, and in vivo evaluation of an inhaled solution of total saponins of *Panax notoginseng* and its protective effect against idiopathic pulmonary fibrosis. *Drug Deliv.* **27** (1), 1718–1728 (2020).
25. Li, H. et al. *Panax notoginseng* saponin alleviates pulmonary fibrosis in rats by modulating the renin-angiotensin system. *J. Ethnopharmacol.* **318**, 116979 (2024).
26. Luo, H. et al. *Panax notoginseng* saponins modulate the inflammatory response and improve IBD-Like symptoms via TLR/NF-[Formula: see text]B and MAPK signaling pathways. *Am. J. Chin. Med.* **49** (4), 925–939 (2021).
27. Zheng, Y., Shao, R., Xia, P., Liang, Z. & Yan, K. Activity and function studies of the promoter cis-acting elements of the key enzymes in saponins biosynthesis of DS from *Panax notoginseng*. *Protoplasma* **259** (1), 163–171 (2022).
28. Zhao, H. et al. Baicalin alleviates bleomycin–induced pulmonary fibrosis and fibroblast proliferation in rats via the PI3K/AKT signaling pathway. *Mol. Med. Rep.* **21** (6), 2321–2334 (2020).
29. Wang, J. et al. Targeting PI3K/AKT signaling for treatment of idiopathic pulmonary fibrosis. *Acta Pharm. Sin B* **12** (1), 18–32 (2022).
30. Nie, Y. et al. S-allyl-l-cysteine attenuates bleomycin-induced pulmonary fibrosis and inflammation via AKT/NF-κB signaling pathway in mice. *J. Pharmacol. Sci.* **139** (4), 377–384 (2019).
31. Andugulapati, S. B., Gourishetti, K., Tirunavalli, S. K., Shaikh, T. B. & Sistla, R. Biochanin-A ameliorates pulmonary fibrosis by suppressing the TGF-β mediated EMT, myofibroblasts differentiation and collagen deposition in in vitro and in vivo systems. *Phytomedicine* **78**, 153298 (2020).
32. Liu, G. et al. Therapeutic targets in lung tissue remodelling and fibrosis. *Pharmacol. Ther.* **225**, 107839 (2021).
33. Phan, T. et al. Emerging cellular and molecular determinants of idiopathic pulmonary fibrosis. *Cell. Mol. Life Sci.* **78** (5), 2031–2057 (2021).
34. Tan, M-M., Chen, M-H., Han, F., Wang, J-W. & Tu, Y-X. Role of bioactive constituents of *Panax notoginseng* in the modulation of tumorigenesis: a potential review for the treatment of cancer. *Front. Pharmacol.* 12, 738914 (2021).
35. Guo, X. et al. *Panax notoginseng* saponins alleviate skeletal muscle insulin resistance by regulating the IRS1-PI3K-AKT signaling pathway and GLUT4 expression. *FEBS Open. Biol.* **9** (5), 1008–1019 (2019).
36. Xie, W. et al. *Panax notoginseng* saponins: a review of its mechanisms of antidepressant or anxiolytic effects and network analysis on phytochemistry and pharmacology. *Molecules* **23** (4), 940 (2018).
37. Ryter, S., Nakahira, K., Haspel, J. & Choi, A. Autophagy in pulmonary diseases. *Annu. Rev. Physiol.* **74**, 377–401 (2012).
38. Zhao, H., Wang, Y., Qiu, T., Liu, W. & Yao, P. Autophagy, an important therapeutic target for pulmonary fibrosis diseases. *Clin. Chim. Acta* **502**, 139–147 (2020).
39. Romero, Y. et al. mTORC1 activation decreases autophagy in aging and idiopathic pulmonary fibrosis and contributes to apoptosis resistance in IPF fibroblasts. *Aging Cell* **15** (6), 1103–1112 (2016).
40. Dehdashtian, E. et al. Diabetic retinopathy pathogenesis and the ameliorating effects of melatonin; involvement of autophagy, inflammation and oxidative stress. *Life Sci.* **193**, 20–33 (2018).
41. Wang, M. et al. Cross-talk between autophagy and apoptosis regulates testicular injury/recovery induced by cadmium via PI3K with mTOR-independent pathway. *Cell Death Dis.* **11** (1), 1–17 (2020).
42. Xu, X., Lai, Y. & Hua, Z. C. Apoptosis and apoptotic body: disease message and therapeutic target potentials. *Biosci. Rep.* **39** (1), BSR20180992 (2019).
43. Hohmann, M. S., Habiel, D. M., Coelho, A. L., Verri, W. A. Jr & Hogaboam, C. M. Quercetin enhances ligand-induced apoptosis in senescent idiopathic pulmonary fibrosis fibroblasts and reduces lung fibrosis in vivo. *Am. J. Respir. Cell Mol. Biol.* **60** (1), 28–40 (2019).
44. Thannickal, V. & Horowitz, J. Evolving concepts of apoptosis in idiopathic pulmonary fibrosis. *Proc. Am. Thorac. Soc.* **3** (4), 350–356 (2006).
45. Kaminskyy, V. O. & Zhivotovsky, B. Free radicals in cross talk between autophagy and apoptosis. *Antioxid. Redox. Signal.* **21** (1), 86–102 (2014).
46. Maiuri, M. C., Zalckvar, E., Kimchi, A. & Kroemer, G. Self-eating and self-killing: crosstalk between autophagy and apoptosis. *Nat. Rev. Mol. Cell Biol.* **8** (9), 741–752 (2007).
47. Song, S., Tan, J., Miao, Y., Li, M. & Zhang, Q. Crosstalk of autophagy and apoptosis: involvement of the dual role of autophagy under ER stress. *J. Cell. Physiol.* **232** (11), 2977–2984 (2017).
48. Wang, K. Autophagy and apoptosis in liver injury. *Cell. Cycle* **14** (11), 1631–1642 (2015).
49. Luo, Z. et al. ROS-induced autophagy regulates Porcine trophectoderm cell apoptosis, proliferation, and differentiation. *Am. J. Physiol. Cell Physiol.* **316** (2), C198–C209 (2019).
50. Huang, F-L., Yu, S-J. & Li, C-L. Role of autophagy and apoptosis in acute lymphoblastic leukemia. *Cancer Control* **28**, 10732748211019138 (2021).
51. Li, X. et al. Duvelisib attenuates bleomycin-induced pulmonary fibrosis via inhibiting the PI3K/Akt/mTOR signalling pathway. *J. Cell. Mol. Med.* **27** (3), 422–434 (2023).
52. Qi, F. et al. LncRNA TUG1 promotes pulmonary fibrosis progression via up-regulating CDC27 and activating PI3K/Akt/mTOR pathway. *Epigenetics* **18** (1), 2195305 (2023).
53. Li, H. et al. *Panax notoginseng* saponin alleviates pulmonary fibrosis in rats by modulating the renin-angiotensin system. *J. Ethnopharmacol.* **318** (Pt B), 116979 (2024).
54. Wang, J. et al. The main bioactive compound of *Panax notoginseng*, notoginsenoside R1, alleviates pulmonary fibrosis via MBD2/SHIP and STAT3 pathway. *J. Funct. Foods* **110**, 105881 (2023).
55. Kanehisa, M., Furumichi, M., Sato, Y., Matsuura, Y. & Ishiguro-Watanabe, M. KEGG: biological systems database as a model of the real world. *Nucleic Acids Res.* **53** (D1), D672–D677 (2025).

Author contributions

Jiong Hou : Writing – original draft, Software, Supervision. Lei Li : Writing – original draft, Software, Supervision. Chun bin Sun : Writing – original draft, Software, Resources. Tian-gang Li : Writing – original draft, Resources. Si qi Zhang : Writing – original draft, Software. Peng tao Liang : Writing – original draft, Software. Yan-ling jin : Writing – original draft, Software. Jia li Yuan : Review & editing. Jin yuan Yan : Review & editing. Li Li : Supervision. Yi Fu : Project administration. Zhong shan Yang : Supervision, Project administration, Funding acquisition.

Funding

This study received support from the National Natural Science Foundation of China (No. 82360017), grants from Yunnan Provincial Science and Technology Department (No.202403AC100007, 202407AB110020, 202005AC160058, 202307AB110046, 202101AZ070001-012, YNWR-QNBJ-2019-069).

Declarations

Competing interests

The authors declare no competing interests.

Additional information

Supplementary Information The online version contains supplementary material available at https://doi.org/10.1038/s41598-025-27541-5.

Correspondence and requests for materials should be addressed to J.-y.Y., Y.F. or Z.-s.Y.

Reprints and permissions information is available at www.nature.com/reprints.

Publisher's note Springer Nature remains neutral with regard to jurisdictional claims in published maps and institutional affiliations.